Proper In deposition amount for on-demand epitaxy of InAs/GaAs single quantum dots*

Xiang-Jun Shang(尚向军)[1,2], Jian-Xing Xu(徐建星)[1,2], Ben Ma(马奔)[1,2], Ze-Sheng Chen(陈泽升)[1,2], Si-Hang Wei(魏思航)[1,2], Mi-Feng Li(李密峰)[1,2], Guo-Wei Zha(查国伟)[1,2], Li-Chun Zhang(张立春)[1,2], Ying Yu(喻颖)[1,2], Hai-Qiao Ni(倪海桥)[1,2], and Zhi-Chuan Niu(牛智川)[1,2,†]

[1] *State Key Laboratory of Superlattices and Microstructures, Institute of Semiconductors, Chinese Academy of Sciences, Beijing* 100083, *China*
[2] *Synergetic Innovation Center of Quantum Information and Quantum Physics, University of Science and Technology of China, Hefei* 230026, *China*

(Received 24 April 2016; revised manuscript received 2 June 2016; published online 25 September 2016)

The test-QD *in-situ* annealing method could surmount the critical nucleation condition of InAs/GaAs single quantum dots (SQDs) to raise the growth repeatability. Here, through many growth tests on rotating substrates, we develop a proper In deposition amount (θ) for SQD growth, according to the measured critical θ for test QD nucleation (θ_c). The proper ratio θ/θ_c, with a large tolerance of the variation of the real substrate temperature (T_{sub}), is $0.964-0.971$ at the edge and >0.989 but <0.996 in the center of a 1/4-piece semi-insulating wafer, and around 0.9709 but <0.9714 in the center of a 1/4-piece N^+ wafer as shown in the evolution of QD size and density as θ/θ_c varies. Bright SQDs with spectral lines at 905 nm–935 nm nucleate at the edge and correlate with individual 7 nm–8 nm-height QDs in atomic force microscopy, among dense 1 nm–5 nm-height small QDs with a strong spectral profile around 860 nm–880 nm. The higher T_{sub} in the center forms diluter, taller and uniform QDs, and very dilute SQDs for a proper θ/θ_c: only one 7-nm-height SQD in 25 μm^2. On a 2-inch (1 inch = 2.54 cm) semi-insulating wafer, by using $\theta/\theta_c = 0.961$, SQDs nucleate in a circle in 22% of the whole area. More SQDs will form in the broad high-T_{sub} region in the center by using a proper θ/θ_c.

Keywords: single quantum dot, proper deposition amount, on-chip distribution, height statistics, μPL spectra

PACS: 78.67.Hc, 81.07.Ta, 78.55.Cr, 73.21.La **DOI:** 10.1088/1674-1056/25/10/107805

1. Introduction

Due to their stable emission[1] and compatibility with GaAs/Al(Ga)As distributed Bragg reflector (DBR) cavity for Purcell enhancement[2] and p–i–n structure for electrical driving,[2–4] InAs/GaAs single quantum dots (SQDs) grown by molecular beam epitaxy and their single photon emission, multiexciton states with spin control,[5,6] and cascade entanglement,[7] cavity quantum electrodynamics,[8,9] and coherence under resonant excitation[10] have attracted great attention. But, the common structures, SQDs embedded in a Fabry–Perot DBR cavity are difficult to grow due to the critical nucleation condition. A low success rate of SQD growth leads to wasting many DBRs, especially expensive high-purity Al source. So, SQD growth must be optimized at first.

The SQD nucleation is sensitive on both the In deposition amount (θ) and the substrate temperature (T_{sub}). Near the critical point, a 0.05-monolayer (ML) change of θ will vary QD density from 0 μm^{-2} to ~ 100 μm^{-2},[11] and a higher T_{sub} will delay the nucleation due to In evaporation. In fact, a tiny variation of the real T_{sub} exists on each substrate, making a constant nominal θ impractical. To raise the success rate, a growth method with large tolerance of the real θ and T_{sub} variation is needed. To tolerate the θ variation, the intrinsic gradient In flux on a static substrate is usually used to grow density-graded QDs, with SQDs forming somewhere definitely[12] but in a small area. Moreover, in recent years, nanowires have been demonstrated to be good platforms (i.e. spatially separated) for SQD formation.[13–15] For large-area SQD growth, a near-uniform distribution of the proper θ on a rotating substrate[16] is more desired. To define the proper θ, the test-QD *in-situ* annealing method was proposed by Li *et al.*,[17] that is, growing test QDs to monitor the critical θ for nucleation (θ_c) by reflection high energy electron diffraction (RHEED), i.e., the point when Bragg spot appears; after *in-situ* annealing, growing formal QDs with θ set according to θ_c (see Fig. 1(c)). This method (i.e., the proper ratio θ/θ_c) allows a large tolerance of the real T_{sub} variation since T_{sub} has the same influence on θ and θ_c; besides, the normal T_{sub} distribution[18–20] keeps a universal relation of the proper θ for SQD nucleation anywhere on chip with the θ_c measured in the center. Apart from its brief application in Ref. [17], there is still much work to do for developing this technique into a practical one for on-demand SQD growth, e.g., finding the proper θ/θ_c locally accounting for the T_{sub} distribution and visualizing the evolution of QD

*Project supported by the National Key Basic Research Program of China (Grant No. 2013CB933304), the Strategic Priority Research Program of Chinese Academy of Sciences (Grant No. XDB01010200), and the National Natural Science Foundation of China (Grant No. 65015196).

†Corresponding author. E-mail: zcniu@semi.ac.cn

© 2016 Chinese Physical Society and IOP Publishing Ltd

nucleation as θ/θ_c varies.

In the present study, based on a long-term growth test (i.e., 19 samples) of InAs/GaAs single quantum dots on rotating substrates by the test-quantum dot *in-situ* annealing method, and systematic multi-point atomic force microscopy (AFM) and micro-photoluminescence (μPL) spectroscopy on each sample, we study the single quantum dot nucleation evolution and on-chip distribution. The higher T_{sub} in the center forms taller, diluter, and uniform quantum dots, and very low-density single quantum dots. Bright single quantum dots with spectral lines at a wavelength of 905 nm–935 nm form at the colder edge, correlated to individual 7 nm–8 nm-height quantum dots in AFM, among 1 nm–5 nm-height dense small quantum dots. The evolutions of quantum dot height and density with θ/θ_c indicate that the proper θ/θ_c values for single quantum dot growth: $0.964 \sim 0.971$ at the edge, > 0.989 but < 0.996 in the center of a 1/4-piece semi-insulating (SI) wafer, and around 0.9709 but < 0.9714 in the center of a 1/4-piece N^+ one, respectively. On a 2-inch SI wafer, by using $\theta/\theta_c = 0.961$, the single quantum dots are distributed in a circle in 22% of the whole area. The proper θ/θ_c discovered here is robust in experiment and enables on-demand single quantum dot growth.

2. Experiments

The samples were grown by Veeco Gen930 MBE on rotating (3 circle/minute) SI or N^+ GaAs (001) substrates. As figure 1(a) shows, the structure consists of GaAs buffer layer, 4 pairs of the bottom GaAs/AlAs DBRs (target wavelength: 920 nm for reflection), test QDs, formal QDs, and surface QDs (for AFM) in GaAs matrix. After growing test QDs to monitor θ_c and *in-situ* annealing at 670 °C for 15 min, the formal QDs were grown with $\theta = \theta_c - \Delta\theta$ ($\Delta\theta$: a setback assumed each time according to the measured θ_c). Many growth tests were performed to estimate the proper $\Delta\theta$. QDs were grown at a relatively high nominal T_{sub}, 540 °C for SI substrate and 490 °C for N^+ substrate, in very low In flux equivalent to a planar rate of 0.005 ML/s, under As_2 pressure of 5×10^{-7} Torr $\sim 7 \times 10^{-7}$ Torr (1 Torr = 1.33322 A·m^{-1}), to allow a slow QD nucleation. For N^+ wafer in good thermal conductivity, the nominal $T_{sub} = 540$ °C cannot form QDs. As tested from 540 °C to a lower one, we found the critical T_{sub} for QD nucleation was 490 °C (see S16 below). GaAs was grown in a rate of 1 μm/h, under As_2 pressure of 3.6×10^{-6} Torr. A 15-s growth interrupt was applied to change As valve before capping QDs. Figure 1(b) shows the QD height statistics. Figure 1(d) shows the fiber-coupled confocal μPL spectrograph.

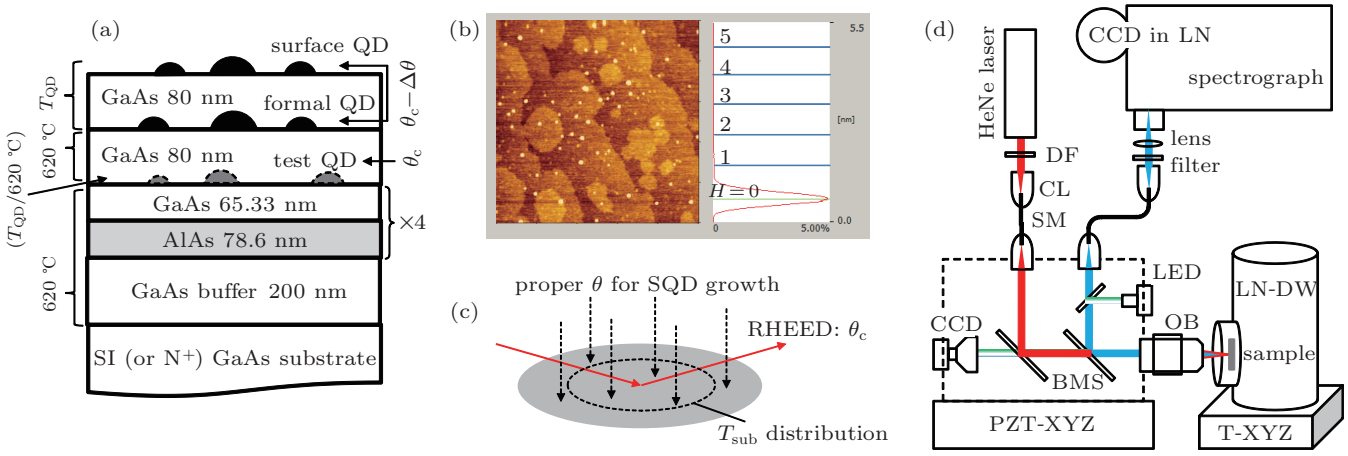


Fig. 1. (color online) (a) Sample structure with T_{sub}. (b) QD height statistics (height is leveled into $H = 1, 2, \ldots$, nm, the baseline (green) is set according to pixel height distribution (red). (c) Test-QD *in-situ* annealing method. (d) Confocal μPL spectrograph. LN-DW: liquid nitrogen (LN)-cooled Dewa (~ 80 K); OB: objective (Miltituyo, 100×, numerical aperture: 0.55, working distance: 13 mm); LED: white light for CCD imaging; DF: density filter; SM: single-mode fiber; CL: focus tunable collimators (Thorlabs); BMS: 50:50 wideband beamspliter (Thorlabs); Dashed rectangular: cage cubes (Thorlabs); Red: HeNe laser ($\lambda = 632.8$ nm) as excitation; Blue: filtered ($\lambda > 800$ nm) luminescence; PZT-XYZ: piezoelectric transition stage; T-XYZ: manual one; CCD in LN: PyLon100; Spectrograph: SP2750 (Princeton Intruments). Attenuated by density filters, the focused laser spot on the sample is ~ 1 μW in power and ~ 2 μm in diameter. It scans the sample by the transition stages for a fast ($t = 1$ s) spectrograph to search SQD spectral lines. The luminescence is collected effectively by the objective and then extracted to the spectrograph by a fiber and collimators.

3. Results and discussion

The ($\Delta\theta$, θ_c) of all samples are shown in Table 1 and Fig. 2. A linear fitting of the success samples with bright SQDs deduces the proper $\Delta\theta$ for SQD formation, $0.0579 \times \theta_c - 0.0483$, valid for $\theta_c = 1.73$ ML–2.31 ML (i.e., a criterion to check whether the T_{sub} distribution is normal). The measured θ_c for test QD nucleation is quite different, due to the real T_{sub} variation, related to conditions of the wafer, the heater non-uniformity, and the substrate holder (e.g. thermal leakage). In some samples, θ_c is as large as 2.8 ML–3.0 ML, due to abnormal high T_{sub} in the center (see discussion below).

Table 1. Sample summary.

No.	Data	θ_c/ML	$\Delta\theta$/ML	T_{QD}/°C	E: edge; C: center; AL: all region; VE: very edge; H: QD height, N: density, (): μPL spectra; –: no nucleation
SI substrate		(1/4-piece wafer as default, except notation)			
1	130416A	–		540	E: $H = 8$–18 nm, $N \sim 20/\mu m^2$
		2.63	0.03	535	C: $H = 1$–7 nm, $N \sim 160/\mu m^2$, (920–1020 nm profile)
2	130425A	2.26	0.01	540	E: $H = 1$–10 nm, $N \sim 300/\mu m^2$, (950–1150 nm broad profile) C: $H = 6$–11 nm for most, $N \sim 120/\mu m^2$
3	130502A	2.23	0.13	540	AL: no QD (no SQD emission)
4	130506A	3.00	0.10	540	E: $H = 9$–17 nm, $N \sim 20/\mu m^2$, (1050–1300 nm broad profile) C: $H = 1$–4 nm, $N \sim 10/\mu m^2$, (no SQD emission)
5	130509A	1.84	0.07	540	E: $H = 1$–6 nm, $N \sim 210/\mu m^2$, (no SQD emission) C: $H = 1$–4 nm, $N \sim 50/\mu m^2$, (no SQD emission)
6	130509B	1.73	0.05	540	E: $H = 1$–8 nm, $N \sim 220/\mu m^2$, (915–935 nm lines, success) C: $H = 1$–4 nm, $N \sim 70/\mu m^2$, (no SQD emission)
7	130831B	1.815	0.04	540	No AFM, AL: (920–980 nm multi peaks, dense QDs) VE: (940 nm single peak, a few QDs)
8	131024A	1.81	0.05	540	E: $H = 1$–10 nm, $N \sim 90/\mu m^2$, (940–1020 nm profile); VE: (910–980 nm lines, SQDs, success 1/2)
9	131102D	2.12	0.07	540	No AFM, E: (905–935 nm lines, SQDs, success)
10	131102E	2.515	0.06	540	No AFM, E: (900–960 nm multi peaks, dense QDs)
11	131118B	1.93	0.07	540	No AFM, E: (900–930 nm lines, SQDs, success)
12	131201C	1.86	0.07	540	No AFM, E: (910 nm weak lines, SQDs, success 1/2)
13	141127A	2.31	0.09	540	No AFM, 2-inch wafer, PIN in DBR cavity, Circle: (930–960 nm lines, SQDs, success)
14	150202A	2.205	0.075	540	No AFM, E: (900–940 nm lines, SQDs, success); C: (no SQD emission)
15	150202B	–		540	No AFM, E: (910 nm weak lines, SQDs, success 1/2)
		2.85	0.11	530	C: (no SQD emission)
N^+ substrate		(1/4-piece wafer as default, except notation)			
16	140123B	–		520	No AFM, above 520 °C, no nucleation;
		2.945[a]		510	a), b) clear nucleation but desorbed during interrupt;
		2.37[b]		500	c) clear nucleation and dotted pattern during interrupt;
		2.09[c]	0.06	490	AL: (940–980 nm profile, dense QDs), nucleate during interrupt
17	140123C	2.06	0.06	490	E: $H = 2$–10 nm, $N \sim 70/\mu m^2$, (920–1020 nm profile); C: $H = 1$–7 nm, $N \sim 176/25/\mu m^2$, (895∼925 nm weak lines, SQDs, success 1/2)
18	140625E	2.1	0.06	490	AL: $H = 8$–13 nm for most, $N = 80 \sim 140/\mu m^2$, (940–1040 nm profile)
19	141118A	2.27	0.05	490	No AFM, 3-inch wafer, PIN in DBR cavity, AL: (1000 nm profile, dense QDs), nucleated at 1.96 ML

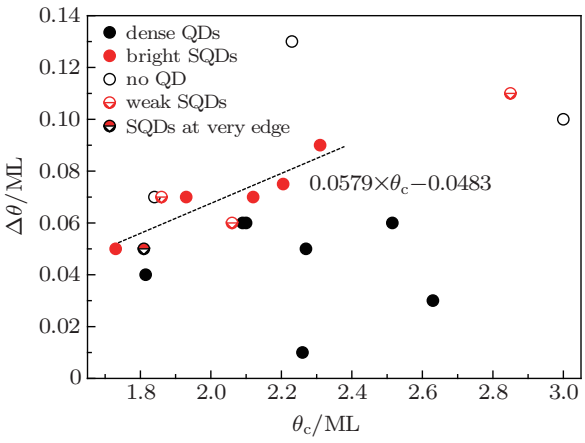


Fig. 2. (color online) ($\Delta\theta$, θ_c) summary. Red: success samples with SQDs; dotted line: linear fitting.

For valid θ_c and proper $\Delta\theta$, as depicted in Fig. 3, SQDs nucleate at the edge of SI wafer (i.e. red circles) and show spectral lines at 905 nm∼935 nm in linewidth of 350 μeV–800 μeV. In S6, QDs at edge points 4 and 6 are in a height of 1 nm–8 nm, in which there are spectral lines; QDs at center points 1 and 2 are in height of 1 nm–5 nm, in which there are no spectral lines. So, SQD spectral lines correspond to individual 7 nm–8 nm-height QDs in AFM. Of course, QD height will reduce after capping due to In–Ga intermixing.[21,22] For valid θ_c but lower $\Delta\theta$, dense QDs form (S2). QDs in the center (point 1, 118 μm^{-2}) have a lower density than QDs at the edge (points 7 and 8, 168 μm^{-2} and 326 μm^{-2}), reflecting a lower T_{sub} at the edge, which enables a prior QD nucleation and non-uniform dense small QD (height: 1 nm–5 nm) formation (see point 8). It is similar for samples on N^+ wafer (S18, see Fig. S12 in Support information). Typically, the T_{sub} fluctuation is 15 °C on a 1/4-piece wafer.[18]

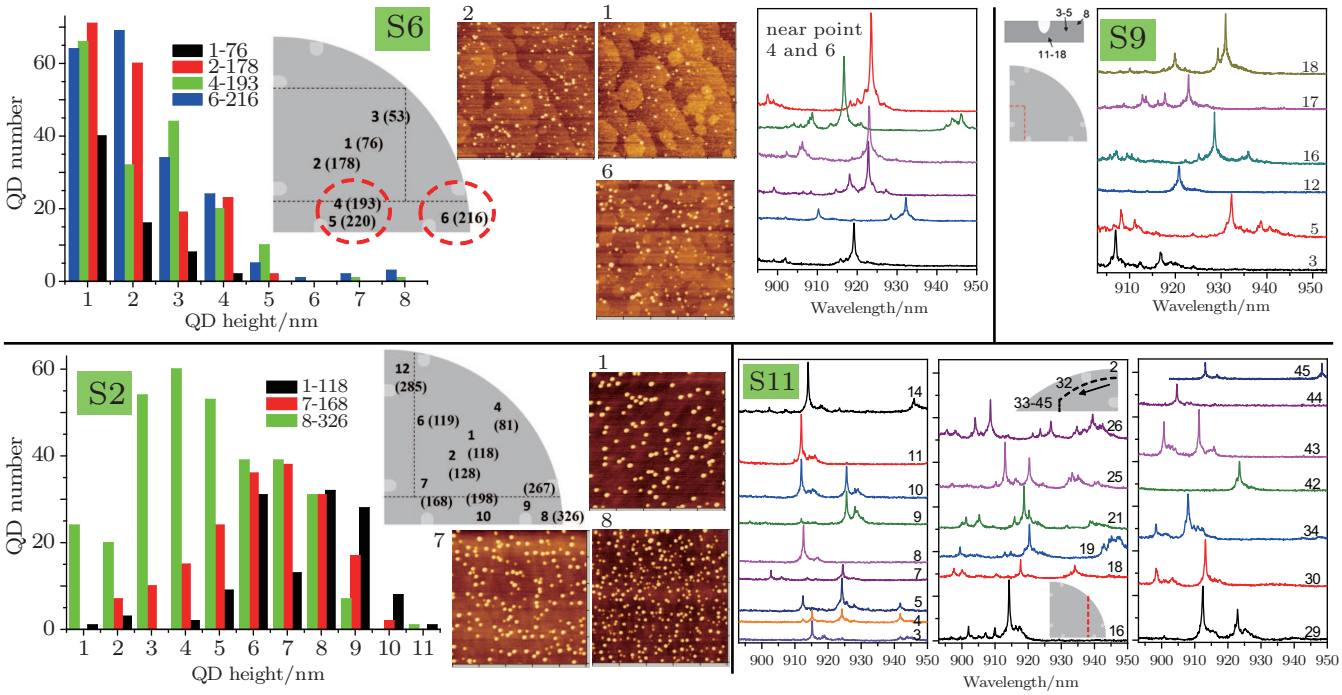


Fig. 3. (color online) SQD on-chip distribution of S6 ($\theta/\theta_c = 0.971$, top left), S9 ($\theta/\theta_c = 0.967$, top right), and S11 ($\theta/\theta_c = 0.964$, bottom right) on SI wafers, described by μPL spectra, 1 μm×1 μm AFM images and QD height statistics. Red circle: SQD region. Bottom left: dense QD on-chip distribution of S2 ($\theta/\theta_c = 0.996$). QD density: in unit of μm^{-2}.

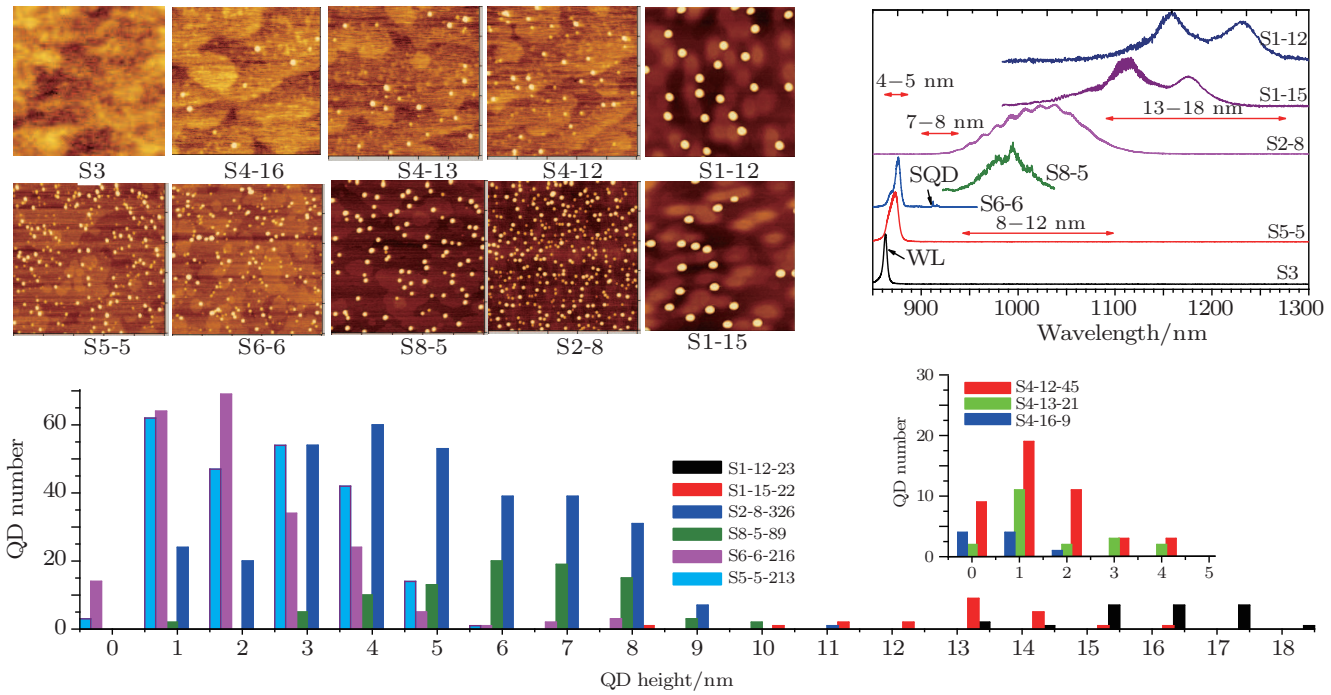


Fig. 4. (color online) Evolutions of QD nucleation at edge. Top right: μPL spectra with corresponding QD height; the rest: 1 μm×1 μm AFM images and QD height statistics. Inset: small QD nucleation, observed in S4 with abnormal T_{sub} distribution (see Support information). Legend name: Sample No.-point No.-QD density [μm^{-2}].

Figure 4 describes the nucleation evolutions with θ/θ_c. It should be noted that the μPL emission mainly comes from the lower transition levels (i.e., larger QDs). For $\theta/\theta_c = 0.942$ (i.e., S3), there is only an InGaAs wetting layer (WL) spectral peak at 863 nm in a width of 5 nm. As θ increases, small QDs appear first; their height rises from 2 nm to 4 nm and their density increases from 9 μm^{-2} to 45 μm^{-2} as observed in S4. As θ/θ_c rises to 0.962 (i.e., S5), the maximal QD height increases to 6 nm and QD density increases to 213 μm^{-2}, with a broad spectral profile around 860 nm∼880 nm, since the previous small QDs become larger and many new 1 nm–3 nm-height small QDs appear. As θ/θ_c rises to 0.971 (i.e., S6), many 3 nm–5 nm-height small QDs are grouped into individual 7 nm–8 nm-height QDs and show spectral lines around

915 nm∼935 nm; the remaining many 1 nm–5 nm-height small QDs show a strong spectral profile around 860 nm–880 nm with two peaks at 876 nm and 868 nm, correlated to the two modes of QD size, 1 nm∼2 nm-height ones and 3 nm∼5 nm-height ones; QD density keeps 216 μm^{-2}. As θ/θ_c reaches 0.972 (i.e., S8) rapidly, most small QDs are grouped into 6 nm–10 nm-height ones and QD density reduces to 89 μm^{-2}; the spectral profile around 940 nm∼1040 nm is from 8 nm∼10 nm-height QDs with sufficiently low transition levels for photocarrier occupation and recombination; the 3 nm∼6 nm-height QDs are nonluminous. In S6, the lower transition levels (i.e., SQD levels) are very fewer than those in S8 and the denser small QDs mainly contribute to the spectrum around 860 nm∼880 nm. As θ/θ_c rises to 0.996 (i.e., S2), many new small QDs with height values of 1 nm–5 nm appear and QD density continues increasing to 326 μm^{-2}; the spectral profile around 950 nm–1100 nm is from 8 nm–11 nm-height QDs with sufficiently low levels for photocarrier occupation. Finally, at the edge of S1 with the nominal θ of 2.6 ML, all small QDs are collected into large ones with height values of 12 nm–18 nm and a density of $\sim 20 \mu m^{-2}$, showing that multi-peak spectral profiles around 1100 nm–1300 nm that are related to QD height distribution.

Figure 5 shows the evolutions of QD density and height with θ/θ_c. The samples with no AFM (i.e., circles) are also presented with QD height assumed to be 7 nm∼10 nm corresponding to their μPL spectra as indicated in Fig. 4. From the success samples with bright SQD spectral lines (i.e., red points), the proper θ/θ_c to form SQDs at the edge of 1/4-piece SI wafers is deduced: in a window of 0.964–0.971, before the rapid jump of QD height (to 10 nm) and drop of QD density (to 89 μm^{-2}) at $\theta/\theta_c = 0.972$. In S12 and S15 ($\theta/\theta_c = 0.961$–0.962, see Fig. S7 and S9 in Support information), SQDs form at very edge with weak spectral lines around 910 nm (success 1/2); in most regions there is no SQD spectrum. In S15, the scanning μPL spectra on chip also reflect the nucleation evolution: large QDs with spectra above 920 nm appear as small QDs grow larger (i.e., the blue-shift of the spectral profile around 860 nm∼880 nm). In S7, S10, and S8 (θ/θ_c = 0.978, 0.976 and 0.972, respectively, see Figs. S4, S6, and S5 in Support information), single spectral peak (S7, S10) or bright SQD spectral lines (S8) only appear at very edge; in most regions we measured, there are many QDs with multi-peak spectral profiles.

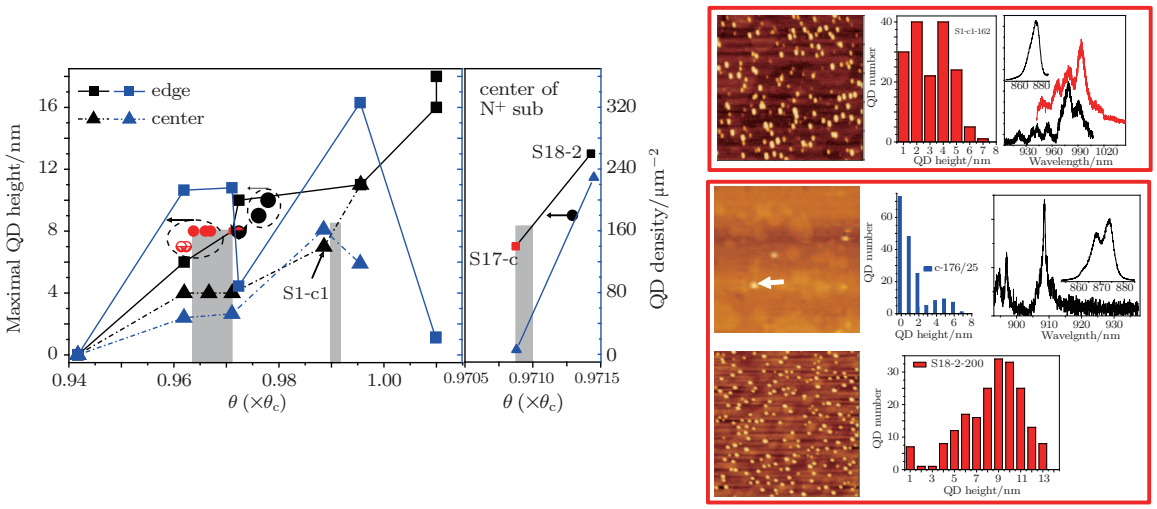


Fig. 5. (color online) Evolutions of QD density and height with θ/θ_c. Left: SI wafers; middle: N^+ ones. Points and left coordinates in black: maximal QD height; points and right coordinates in blue: QD density. Circle points: Assumed QD height of samples with no AFM; red: SQDs; black: dense QDs. Grey regions: proper θ/θ_c. Right: 1 μm×1 μm AFM images, QD height statistics and μPL spectra of S1-c1, S17-c, and S18-2. For more details, see Support information.

The abnormal high θ_c is due to a novel high T_{sub} in the center. In this case, the proper θ/θ_c is no longer valid (see Support information. In S1 ($\theta_c = 2.63$ ML, $\theta/\theta_c = 0.989$, see Fig. S1), large QDs with height values of 10 nm–18 nm form in all regions at the edge; in S4 ($\theta_c = 3.0$ ML, $\theta/\theta_c = 0.967$, see Fig. S2), large QDs with height values of 9 nm–17 nm form in some regions at the edge while small QDs or no QDs form in the other regions at the edge; in S15 ($\theta_c = 2.85$ ML, $\theta/\theta_c = 0.961$, see Fig. S9), SQDs with weak spectral lines around 910 nm form at very edge.

In the center of SI wafer, $\theta/\theta_c = 0.962$ (point 3 in S5) and 0.971 (point 3 in S6) forms QDs in height of 1 nm–4 nm and density of $\sim 50 \mu m^{-2}$. $\theta/\theta_c = 0.989$ (point c1 in S1) forms QDs with height of 1 nm–7 nm and a density of 162 μm^{-2}, with multi-peak spectra at 920 nm–1020 nm; the flat QD height distribution in 1 nm–4 nm contributes to a broad spectral profile around 860 nm∼880 nm, in similar shape to the case at point 5 in S5. A jump of QD height (to 11 nm)

and drop of QD density (to 118 μm^{-2}) occur at $\theta/\theta_c = 0.996$ (point 4 in S2). So, the proper θ/θ_c to obtain SQDs is > 0.989 but < 0.996.

For samples on 1/4-piece N^+ wafers, in the center, $\theta/\theta_c = 0.9709$ (S17) forms dilute QDs (176/25 μm^{-2}) and the SQDs with height of 7 nm are only 1 in 25 μm^{-2} as indicated in AFM image (see Fig. S11 in Support information), showing weak spectral lines around 910 nm, most QDs have height of 0 nm–2 nm and only a few have height of 3 nm–6 nm, consistent with the two-peak spectral profile around 860 nm–880 nm; $\theta/\theta_c = 0.9714$ (point 2 in S18) forms QDs height of 1 nm–13 nm and density of 200 μm^{-2}. So, the proper θ/θ_c for SQD nucleation is around 0.9709 but < 0.9714. QD nucleation is very sensitive to θ/θ_c. In S16 ($\theta/\theta_c = 0.9713$), above 520 °C, no test QDs nucleate. At 510 °C and 500 °C, test QDs nucleate at $\theta_c = 2.945$ and 2.37 ML respectively and desorb quickly during growth interrupt. At 490 °C, test QDs nucleate at $\theta_c = 2.09$ ML, formal QDs nucleate at $\theta = 2.03$ ML and become dense quickly. The ultra-low density SQDs, the rapidly varying QD nucleation at different values of T_{sub}, and the near-uniform θ_c at the same T_{sub} reflect the good thermal conductivity of N^+ wafer which enhances both In diffusion and In evaporation.

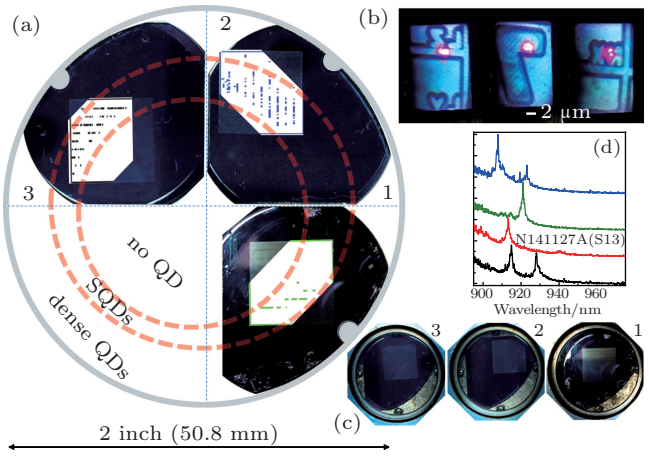


Fig. 6. (color online) (a) SQD distribution on a 2-inch SI wafer, dots: SQD regions. (b) CCD imaging of grid marks during μPL. (c) 1/4 pieces in Dewa. (d) μPL spectral lines.

Then, we use $\theta/\theta_c = 0.961$ to grow SQDs on a 2-inch SI wafer, i.e., S13, a p-i-n structure with SQDs in 1–λ cavity between 4 pairs of the top DBRs and 10 pairs of the bottom ones. 2-μm-wide grid marks are fabricated by photolithograph and wet-etching; their CCD imaging during μPL (Fig. 6(b)) records the locations of SQD regions (i.e., dots in Fig. 6(a)). SQDs with spectral lines around 910 nm (Fig. 6(d)) are distributed in a circle in 22% of the whole area, sandwiched between a broad non-QD region (center, higher T_{sub}) and a dense-QD region (edge, lower T_{sub}). It is consistent with the fact that $\theta/\theta_c = 0.961$ only forms SQDs at very edge of a 1/4-piece SI wafer. The broad non-QD region in the center reflects a near-uniform T_{sub} distribution there[18] and near-uniform θ distribution.[16] To increase SQD regions on the 2-inch wafer, a proper θ/θ_c for SQD nucleation in the center (> 0.989 and < 0.996) is desired. The broad SQD spectral lines are due to a strong tunneling under the built-in electric field.[12,23] In fact, these spectral lines occur on grid marks where the front P^+ region has been etched (that reduces the built-in field).

4. Conclusions

In this work, by using the test-QD *in-situ* annealing method to optimize InAs/GaAs single quantum dot (SQD) epitaxy on rotating substrates with near-uniform In deposition amount (θ) distribution, we develop a proper θ for on-demand SQD growth, according to the measured critical θ for test QD nucleation (θ_c). The evolutions of QD height and density with θ/θ_c indicate the proper θ/θ_c for SQD nucleation. On a 1/4-piece SI wafer, it is in a window of 0.964–0.971 at the edge and > 0.989 but < 0.996 in the center; on a 1/4-piece N^+ wafer, it is around 0.9709 but < 0.9714 in the center, quite sensitive to θ. At the higher substrate temperature (T_{sub}) in the center form diluter, taller and uniform QDs, and very low-density SQDs (only 1 in 25 μm^{-2}); while the lower one at the edge enables a prior QD nucleation and non-uniform dense QD formation. Bright SQDs with spectral lines at 905 nm–935 nm nucleate at the colder edge and are correlated to 7 nm–8 nm-height QDs in AFM. On a 2-inch SI wafer, by using $\theta/\theta_c = 0.961$, SQDs nucleate in a circle in 22% of the whole area. A proper θ/θ_c for SQD nucleation in the center will increase SQD regions on the 2-inch wafer.

Acknowledgment

We thank Yu-Ming He, Zhao-Chen Duan and Prof. Chao-Yang Lu in University of Science and Technology of China for honest guide on confocal spectrograph setup, Wei-Hong Yin and Prof. Xiao-Hong Yang in State Key Laboratory on Integrated Optoelectronics, Institute of Semiconductors (IOS), Chinese Academy of Sciences (CAS), for $>$ 1000 nm μPL spectroscopy with HORIBA LabRAM HR800, and De-Song Wang in Engineering Research Center for Semiconductor Integrated Technology, IOS, CAS, for photolithograph.

References

[1] Konthasinghe K, Peiris M, Yu Y, Li M F, He J F, Wang L J, Ni H Q, Niu Z C, Shih C K and Muller A 2012 *Phys. Rev. Lett.* **109** 267402
[2] Heindel T, Schneider C, Lermer C, Kwon S H, Braun T, Reitzenstein S, Höfling S, Kamp M and Forchel A 2010 *Appl. Phys. Lett.* **96** 011107
[3] Patel R B, Bennett A J, Farrer I, Nicoll C A, Ritchie D A and Shields A J 2010 *Nat. Photon.* **4** 632
[4] Dou X M, Chang X Y, Sun B Q, Xiong Y H, Niu Z C, Huang S S, Ni H Q, Du Y and Xia J B 2008 *Appl. Phys. Lett.* **93** 101107
[5] Yamaguchi M, Asano T and Noda S 2012 *Rep. Prog. Phys.* **75** 096401
[6] He Y, He Y M, Wei Y J, Jiang X, Chen M C, Xiong F L, Zhao Y, Schneider C, Kamp M, Hofling S, Lu C Y and Pan J W 2013 *Phys. Rev. Lett.* **111** 237403

[7] Wu X F, Dou X M, Ding K, Zhou P Y, Ni H Q, Niu Z C, Zhu H J, Jiang D S, Zhao C L and Sun B Q 2015 *Chin. Phys. Lett.* **32** 124204
[8] Ye H, Peng Y W, Yu Z Y, Zhang W and Liu Y M 2015 *Chin. Phys. B* **24** 114202
[9] Zhang W and Lu H T 2015 *Chin. Phys. B* **24** 067806
[10] Ates S, Ulrich S M, Reitzenstein S, Loffler A, Forchel A and Michler P 2009 *Phys. Rev. Lett.* **103** 167402
[11] Placidi E, Arciprete F, Fanfoni M, Patella F and Balzarotti A 2008 *The InAs/GaAs* (001) *Quantum Dots Transition: Advances on Understanding, Self-Assembled Quantum Dots* (Chapter 1) (New York: Springer) p. 6
[12] Yu Y, Shang X J, Li M F, Zha G W, Xu J X, Wang L J, Wang G W, Ni H Q and Niu Z C 2013 *Appl. Phys. Lett.* **102** 201103
[13] Yu Y, Li M F, He J F, He Y M, Wei Y J, He Y, Zha G W, Shang X J, Wang J, Wang L J, Wang G W, Ni H Q, Lu C Y and Niu Z C 2013 *Nano Lett.* **13** 1399
[14] Yu Y, Dou X M, Wei B, Zha G W, Shang X J, Wang L, Su D, Xu J X, Wang H Y, Ni H Q, Sun B Q, Ji Y, Han X D and Niu Z C 2014 *Adv. Mater.* **26** 2710
[15] Yang S, Dou X M, Yu Y, Ni H Q, Niu Z C, Jiang D S and Sun B Q 2015 *Chin. Phys. Lett.* **32** 077804
[16] Shiralagi K T, Kriman A M and Maracas G N 1991 *J. Vac. Sci. Technol. A* **9** 65
[17] Li M F, Yu Y, He J F, Wang L J, Zhu Y, Shang X J, Ni H Q and Niu Z C 2013 *Nanoscale Res. Lett.* **8** 86
[18] Fang X M, Yurasits T R, Loubychev D, Wu Y, Liu W K, DeBruzzi M, Priddy S and Schiprett C 2001 *J. Vac. Sci. Technol. B* **19** 1554
[19] Jacksona A W and Gossard A C 2007 *J. Crystal Growth* **301–302** 105–108
[20] Nagai M, Matsumoto K, Morishima M, Hone H, Niwata Y and Hayakawa T 1993 *J. Crystal Growth* **127** 54
[21] García J M, Medeiros-Ribeiro G, Schmidt K, Ngo T, Feng J L, Lorke A, Kotthaus J and Petroff P M 1997 *Appl. Phys. Lett.* **71** 2014
[22] Eisele H, Lenz A, Heitz R, Timm R, Dähne M, Temko Suzuki Y T and Jacobi K 2008 *J. Appl. Phys.* **104** 124301
[23] Shang X J, Yu Y, Zha G W, Li M F, Wang L J, Xu J X, Ni H Q and Niu Z C 2013 *J. Phys. D: Appl. Phys.* **46** 405102